Journal of Quantitative Spectroscopy & Radiative Transfer ▮ (▮▮▮▮) ▮▮▮–▮▮▮

Contents lists available at ScienceDirect

Journal of Quantitative Spectroscopy & Radiative Transfer

journal homepage: www.elsevier.com/locate/jqsrt

Effect of polarization on dual-band infrared metamaterial emitters or absorbers

Atsushi Sakurai [a,b], Bo Zhao [a], Zhuomin M. Zhang [a,*]

[a] George W. Woodruff School of Mechanical Engineering, Georgia Institute of Technology, Atlanta, GA 30332, USA
[b] Department of Mechanical and Production Engineering, Niigata University, 8050, Ikarashi 2-no-cho, Niigata 950-2181, Japan

ARTICLE INFO

Article history:
Received 17 September 2014
Received in revised form
26 November 2014
Accepted 28 November 2014

Keywords:
Absorptance
Emittance
Metamaterials
Nanostructures
Polarization effect

ABSTRACT

This work deals with the spectral radiative properties of metamaterials made of a 2D metallic pattern on a dielectric thin film that separates the top periodic structure from a metal ground plane. Two distinct patterns are considered: one consists of disconnected double-rectangle gold pattern and the other is made of L-shape pattern. Both structures exhibit dual-band emission or absorption peaks in the infrared region. Unlike the disconnected rectangular pattern for which the normal emittance is independent of the polarization angle, the L-shape structure shows strong polarization dependent due to near-field coupling. The electromagnetic fields at the resonant frequencies are analyzed using the finite-difference time-domain technique to elucidate the physical mechanisms accounting for the different behaviors. For both structures, the resonance mechanisms can be explained by magnetic polaritons. Inductor–capacitor circuit models are developed to quantitatively predict the resonance frequencies. This work helps the understanding of polarization dependence in metamaterials and may facilitate their applications in biosensing and infrared spectroscopic system.

1. Introduction

Electromagnetic metamaterials refer to a class of engineered artificial structures containing periodic patterns of (usually) metallic elements with geometric features smaller than the wavelength. Exotic and superior optical, thermal radiative, or microwave characteristics, which are absent or rarely exit in natural materials, have been demonstrated using metamaterials [1–3]. Recently, metamaterial emitters or absorbers with a metal–insulator–metal structure have attracted much attention [4–8]. Specifically, wavelength-selective infrared absorption or emission shows promising biosensing applications due to the infrared vibrational fingerprints of biomolecules that can be applied for their identification [9]. To meet the requirement for various applications, single-band, dual-band, and multi-band emitters and absorbers have been demonstrated. For example, polarization and angular insensitive near-perfect absorbers have been developed in the near infrared for plasmonic sensing with a single-band response [10]. Liu et al. [4] demonstrated dual-band and multi-band mid-infrared emitters using cross-shape patterns with different sizes. Zhang et al. [11] fabricated elliptical nanodisks, with a 90° rotation between two adjacent disks, to realize dual-band near-perfect absorption. Tao et al. [12] observed two absorption peaks in the far-infrared region based on the electric-field-coupled resonators. These metamaterial absorbers or emitters are designed for polarization-independent response. However, some metamaterial absorbers or emitters exhibiting polarization control ability are also attractive for practical applications where polarization selectivity is desired [13–17].

* Corresponding author.
E-mail address: zhuomin.zhang@me.gatech.edu (Z.M. Zhang).

http://dx.doi.org/10.1016/j.jqsrt.2014.11.018
0022-4073/

Please cite this article as: Sakurai A, et al. Effect of polarization on dual-band infrared metamaterial emitters or absorbers. J Quant Spectrosc Radiat Transfer (2015), http://dx.doi.org/10.1016/j.jqsrt.2014.11.018

Although polarization-dependent radiative properties of asymmetric metamaterials have been observed [18–20], the near-field coupling in these structures has not been fully investigated. Further studies on the resonant mechanisms and coupling effects in metamaterial absorbers or emitters are necessary in order to better understand their polarization sensitivity to assist future design tailored toward specific applications.

The present study deals with two patterns that support magnetic resonances for dual-band emission or absorption peaks. A comparative study of the two metamaterial designs with different polarization dependences is performed. Both designs consist of a three-layer metamaterial structure with a metal (gold) pattern, a dielectric (Al_2O_3) film, and a gold ground plane. The difference lies in that unit cell of the top layer has different gold patterns. One of the structures is made of two separate gold rectangles and the other is constructed by connecting the two rectangles to form an L-shape pattern. The former structure shows polarization-independent radiative properties, while the latter exhibits strong polarization dependence. The objective of this study is to explore the underlying mechanisms that result in either polarization-dependent or polarization-independent radiative properties near the magnetic resonance or magnetic polariton (MP) wavelengths. The finite-difference time-domain (FDTD) technique is employed to calculate the radiative properties and the electromagnetic field distributions, which are then used to elucidate the resonance mechanism and to scrutinize the near-field coupling effect. Furthermore, the inductor–capacitor (LC) circuit model is developed for each structure considering the different geometries following the field distributions to quantitatively predict the MP frequencies.

2. Metamaterial structures and numerical method

Fig. 1 shows a unit cell of the double-rectangle and L-shape metamaterial emitters or absorbers. Gold patterns are placed over a dielectric film or spacer (Al_2O_3) on a ground plane made of a gold film that is thick enough to be treated as opaque. In the following, the rectangular pattern whose long side is along the *y*-direction is called the *vertical rectangle*, and the one along the *x*-direction is called the *horizontal rectangle*. The geometric parameters include period Λ, thickness of gold patterned layer h, thickness of dielectric layer d, long-side length w_1, short-side length w_2, and distances between the edge of the gold pattern and cell boundary s_1 and s_2. The parameters used for both metamaterial structures are listed in Table 1.

The FDTD method (Lumerical Solutions, Inc.) is used for calculating the infrared reflectance of the two metamaterial emitters and absorbers by solving the Maxwell equations. The optical constants of gold and Al_2O_3 are obtained from Palik [21]. For simplicity and ease of revealing the underlying mechanisms, the refractive index of Al_2O_3 is assumed to be constant according to $n=1.57$ at the wavelength $\lambda=6.25$ μm. In practice, Al_2O_3 becomes dispersive at wavelengths beyond 8 μm, resulting in a drop of the refractive index along with an increased absorption. Although the effect of the dispersive behavior should be taken into account for more realistic simulation, the focus of the present study is on elucidating the underlying mechanisms and therefore Al_2O_3 is treated as a lossless nondispersive dielectric. A unit cell of the considered structure is calculated using periodic boundary conditions

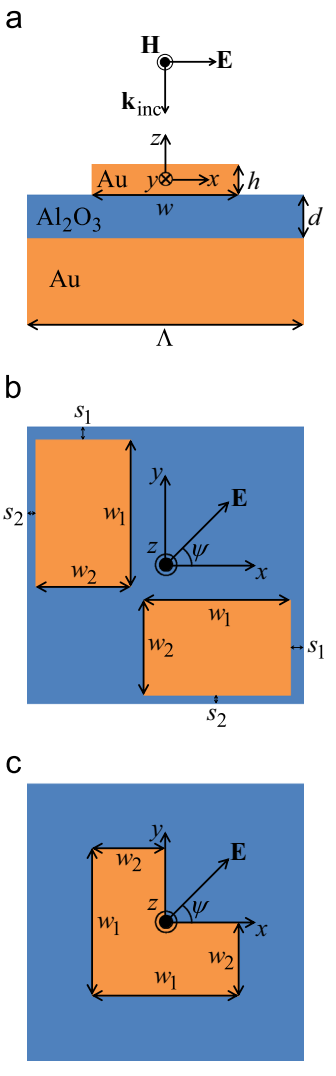

Fig. 1. Schematic of the metamaterial emitter and absorber. (a) Side view of the three-layer structure, also showing the incident wavevector $\mathbf{k}_{inc}$ and polarization angle; (b) top view of the double-rectangle pattern; (c) top view of the L-shape pattern. Note that gold (Au) is used for the metallic patterns and the ground plane, and Al_2O_3 is used for the dielectric film or spacer.

Table 1
Geometric parameters for the metamaterial structure used in the present study.

Period	Λ [μm]	3.2
Thickness of top metallic pattern	h [nm]	100
Thickness of dielectric spacer	d [nm]	140
Length of long side	w_1 [μm]	1.7
Length of short side of rectangle	w_2 [μm]	1.1
Length of short side of L-shape	w_2 [μm]	0.85
Length of margin	s_1 [μm]	0.15
Length of margin	s_2 [μm]	0.10

Please cite this article as: Sakurai A, et al. Effect of polarization on dual-band infrared metamaterial emitters or absorbers. J Quant Spectrosc Radiat Transfer (2015), http://dx.doi.org/10.1016/j.jqsrt.2014.11.018

along both x and y directions. A perfectly matched layer is assumed along the propagation direction (z-direction since only normal incidence is considered). The plane of incidence is parallel to the x–z plane, and the polarization angle ψ is defined, as shown in Fig. 1, such that the transverse magnetic (TM) wave and the transverse electric (TE) wave are at $\psi=0^\circ$ and 90°, respectively. A frequency domain power monitor is placed above the plane wave source to detect the reflected waves. According to Kirchhoff's law [22], spectral-directional emittance ε_λ is equal to spectral-directional absorptance α_λ, which is equal to $1-R_\lambda$ since the metamaterial structure is opaque. Normal specular reflectance R_λ is simulated from the FDTD. All of the FDTD simulations in this study are performed in 3D computational domain. It takes approximately 1 h to run a full spectral calculation for a certain polarization on a dual eight core XEON E5-2687W workstation with all the processors running in parallel.

3. Results and discussion

3.1. Polarization independence of metamaterial

The normal spectral emittance for both structures is shown in Fig. 2. It can be seen that emittance for the double-rectangle patterned metamaterial is enhanced significantly around $\lambda=4.72$ μm and 6.67 μm and the emittance is independent of the polarization angle. On the other hand, the polarization effects can be observed in Fig. 2b for the L-shape patterned metamaterial. Note that the curves for the cases $\psi=0^\circ$ and 90° overlap but the other curves show distinct differences, even for 45° and 135° polarization angles. The emittance peak for the resonance at the longer wavelength shows up for $\psi=45^\circ$ but disappears when $\psi=135^\circ$. The reverse is true for the resonance at the shorter wavelength where the emittance peak occurs for $\psi=135^\circ$ but disappears when $\psi=45^\circ$. The following focuses on the case of the double-rectangle patterned metamaterial. The L-shape patterned metamaterial will be discussed in Section 3.2.

Similar to the structure for which the unit cell has just one single rectangular pattern, the physical mechanism responsible for the wavelength-selective emission and absorption in the double-rectangle pattern can be explained as due to the excitation of MPs [7,8,23–25]. As shown in Fig. 3, the electric and magnetic fields of the double-rectangle patterned structure are visualized with $\psi=0^\circ$ at the cross-section along the x–z plane in the middle of the vertical and horizontal rectangles, respectively, at the corresponding resonance wavelength. The contour indicates the strength of the resulting magnetic field normalized to the incident, and the vectors represent the direction and magnitude of electric field. The magnetic field inside the dielectric spacer is greatly enhanced, indicating the diamagnetism response. The oscillating antiparallel currents can be induced by the time-varying magnetic field and a closed current loop can be formed [8] around the enhanced magnetic field at the resonance wavelengths. This characteristic of electromagnetic field distribution shows excitation of magnetic resonance or MPs.

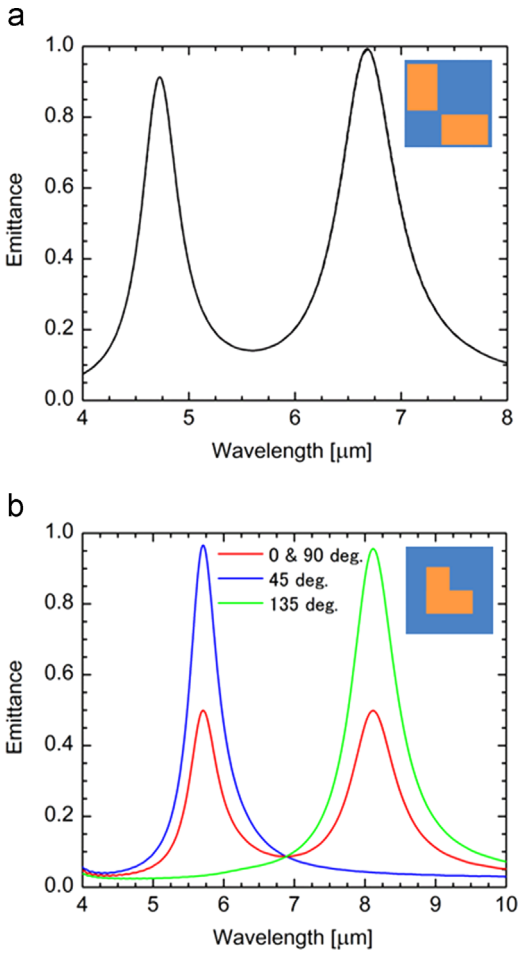

Fig. 2. Normal spectral emittance for (a) the structure with double-rectangle gold pattern, which is independent of the polarization angle ψ, and (b) the structure with L-shape pattern for different ψ. Note that curves for $\psi=0^\circ$ and 90° overlap with each other.

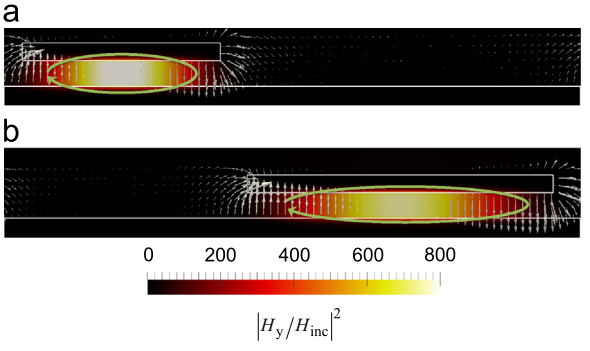

Fig. 3. Electromagnetic field profile at the resonant wavelength at $\psi=0^\circ$: (a) $\lambda=4.72$ μm where the resonance is under the horizontal rectangle; (b) $\lambda=6.67$ μm where the resonance is under the vertical rectangle. The contour shows the relative magnitude of the y-component of the magnetic field. The arrows show the direction and magnitude of the electric field.

Fig. 4 shows the magnetic field profile in the x–y plane at the middle of the dielectric spacer. As shown in Figs. 4a and 4b, when MPs are excited under TM-wave incidence

Please cite this article as: Sakurai A, et al. Effect of polarization on dual-band infrared metamaterial emitters or absorbers. J Quant Spectrosc Radiat Transfer (2015), http://dx.doi.org/10.1016/j.jqsrt.2014.11.018

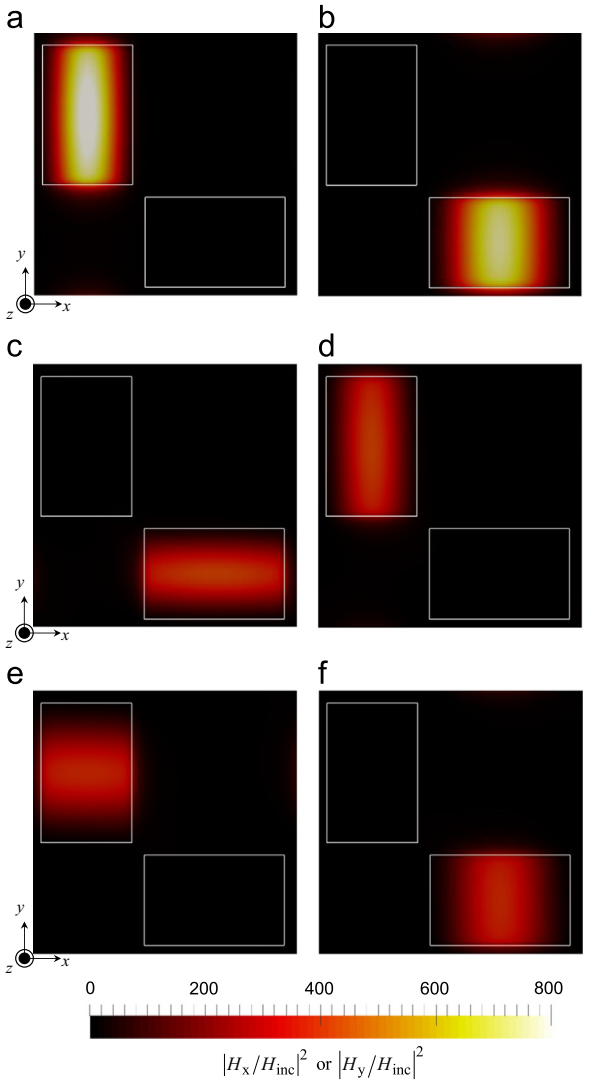

Fig. 4. Magnetic field profile in the middle plane of the dielectric spacer. (a,b) The y-component for $\psi=0^\circ$ at $\lambda=4.72$ μm and $\lambda=6.67$ μm, respectively; (c–f) $\psi=45^\circ$ with $\lambda=4.72$ μm in (c and d) and $\lambda=6.67$ μm in (e and f). Note that (c and e) are for the x-component, while (d and f) are for the y-component of the magnetic field. The contour shows the square magnitude of the magnetic field relative to the incidence and all figures used the same scale bar at the bottom.

($\psi=0^\circ$), the field enhancement only occurs under the vertical and horizontal rectangles at the resonant wavelength $\lambda=4.72$ μm and 6.67 μm, respectively. For TE-wave incidence ($\psi=90^\circ$), since it can be viewed as TM-wave incidence with a 90° rotation of the x–y plane along the z-axis, the result is simply the interchange of the field enhancement between the two rectangles and the magnetic field is changed from the y direction to the x direction. However, for other polarization angles, the field enhancement locations will not be the same, though the absorptance is polarization-independent. Fig. 4b–f shows the x- and y-components of the magnetic field for the polarization angle $\psi=45^\circ$. For the MP resonance at $\lambda=4.72$ μm, the x-component of magnetic field excites the MP under the horizontal rectangle (Fig. 4c), and the y-component of magnetic field excites the MP under the vertical rectangle (Fig. 4d) simultaneously. Because the incoming magnetic field is split into two directions, the field strength is not as strong as in Fig. 4a and b. Since the enhancement of the magnetic field in both directions contributes to the absorption, the overall absorptance is the same as for $\psi=0^\circ$. Similarly, for resonance at $\lambda=6.67$ μm, the x-component of magnetic field excites the MP under the vertical rectangle (Fig. 4e), and the y-component of magnetic field excites the MP under the horizontal rectangle (Fig. 4f) simultaneously, and they contribute equally to the absorption enhancement. For other polarization angles, the field enhancement is unevenly distributed to these two patterns at the MP resonance wavelength, although not shown. It is interesting to note that while the macroscopic far-field radiative properties are independent of the polarization angle. The near-field power dissipation or absorption distribution is very different. The difference may be employed for local selective heating with a spatial resolution on the order of 1 μm. These two rectangular patterns are separated and, therefore, there is no field coupling between each other, resulting in the dual peaks that are independent of the polarization angle. Note that the MP resonance at $\lambda=4.72$ μm is associated with the length of the short side w_2 of the rectangular pattern and the MP resonance at $\lambda=6.67$ μm depends on the length of the long side w_1, which can be explained with an LC model as discussed next.

The circuit model has been successfully applied to predict magnetic resonance conditions for nanostructures [26–30]. Especially, our previous work [29] focuses on the development of a RLC circuit model and the structure considered has only one emission peak. The RLC circuit model includes the effect of resistance so that it can predict both the resonance wavelength and the shape of emission spectra. The present study aims at investigating the different polarization mechanisms of the different patterns. For simplicity, the LC circuit model shown in Fig. 5 is used to explain the MP resonances for each structure considering the different geometries. When MPs are excited, electromagnetic field is strongly confined between the top metallic structure and the bottom metallic film. Therefore, the considered structure can be assumed to be metal strip pairs although a thick bottom metallic film is used. For the double-rectangle patterned metamaterial, the MPs can be excited independently for each rectangle. The total impedance for the LC circuit as shown in Fig. 5 can be expressed as

$$Z_{tot}(\omega)=2\left(\frac{1}{\omega^2 C_m}+L_k+L_m\right) \quad (1)$$

where L_m is the magnetic inductance or mutual inductance, which is originated from the magnetic energy stored in the dielectric spacer of distance d between the two parallel plates. L_k is the kinetic inductance, which is originated from the kinetic energy of the electrons inside the metal. The dielectric that separates top metal structure and the ground plate serves as a capacitor and a capacitance C_m is considered. Gap capacitance which describes the capacitance of the air gap between the neighboring patterns is negligibly small compared to C_m and thus is not

Please cite this article as: Sakurai A, et al. Effect of polarization on dual-band infrared metamaterial emitters or absorbers. J Quant Spectrosc Radiat Transfer (2015), http://dx.doi.org/10.1016/j.jqsrt.2014.11.018

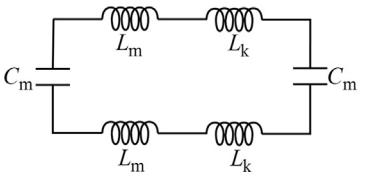

Fig. 5. Schematic of the equivalent LC circuit for both structures. Note that the parameter modeling is different for the two structures as discussed in the text.

included in the model. These four parameters are defined as [30]

$$L_m = \frac{1}{2}\mu_0 \frac{wd}{l},\ L_k = -\frac{w}{\varepsilon_0 \omega^2 l \delta} \frac{\varepsilon'}{(\varepsilon'^2 + \varepsilon''^2)},\ \text{and}$$

$$C_m = c' \varepsilon_d \varepsilon_0 \frac{wl}{d} \tag{2}$$

where w and l are the characteristic lengths perpendicular and parallel to the main stream of magnetic field, respectively. Penetration depth of the electric field $\delta = \lambda/2\pi\kappa$, where κ is the extinction coefficient, is introduced. Also, an optimized parameter c' represents the fringe effect or non-uniform charge distribution along the surface of capacitor and can be varied between 0.2 and 0.3 [27]. The resonance wavelength can be obtained by zeroing the total impedance in Eq. (1). For the resonant wavelength $\lambda = 4.72$ μm, the MP is mainly excited by the short side, therefore, the optimized parameters c' can be obtained as 0.279 with $w = w_2$ and $l = w_1$. For the resonant wavelength $\lambda = 6.67$ μm, the MP is mainly excited by the long side, therefore, the optimized parameters c' can be obtained as 0.234 with $w = w_1$ and $l = w_2$. Note that the predicted resonance wavelengths are independent of length l since it is canceled out in the LC model. Consequently, the predicted MP resonance wavelengths agree well with the FDTD simulation.

3.2. Polarization-dependent metamaterial

The strong polarization effects shown in Fig. 2 can be clearly seen in Fig. 6 for the L-shape patterned metamaterial, especially at the wavelength when either of the resonances is excited. The first and second resonances are at $\lambda = 5.70$ μm and 8.13 μm, respectively. The emittance of TE and TM waves are identical for normal incidence for any wavelength due to the symmetry of the structure, which can be also observed in Fig. 6 at $\psi = 0°$, 90°, and 180°. Both of the emittance peaks show up in the spectrum at these polarization angles. However, at $\psi = 45°$, only the peak at $\lambda = 5.70$ μm occurs, while at $\psi = 135°$, only the peak at $\lambda = 8.13$ μm, which shows strong polarization dependence.

The instantaneous electromagnetic field distributions are shown in Fig. 7 in order to explain the effect of polarization for the L-shape pattern metamaterial. These electromagnetic field profiles are for the plane in the middle of dielectric spacer at the resonant wavelength under illuminations of different incidence with varying polarization angles. The magnitudes of incident electric wave are all unit. The contour shows the z component of the electric field normalized by the magnitude of the

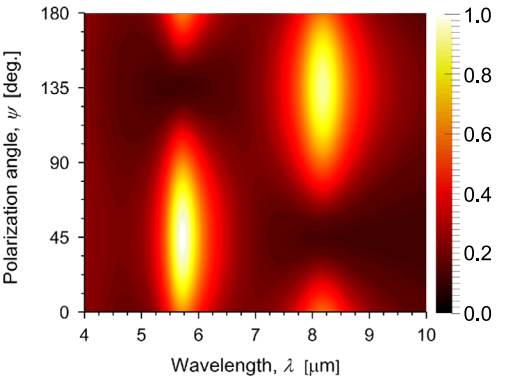

Fig. 6. Normal emittance contour for the L-shape patterned metamaterial.

incident electric field and the vectors show the direction and magnitude of the magnetic field. Also, the length of the arrows indicates the magnitude of the instantaneous magnetic field and the scale bar for the magnetic fields is the same for all plots. The wavelengths of incidence are $\lambda = 5.70$ μm and 8.13 μm in Fig. 7a–d and Fig. 7e–h, respectively. Also, the polarization angles are 0°, 45°, 90°, and 135°. Although it does not show here, the case for polarization angle $\psi = 180°$ was calculated, and the fields are pointing to the opposite direction at each space point for both the electric and magnetic field as compared with the case for $\psi = 0°$, since $\psi = 180°$ can be treated as $\psi = 0°$ with an additional π phase delay. It clearly shows that the magnetic fields in Figs. 7a and 7c are generally pointing to the same direction. Since the electromagnetic field at $\psi = 45°$ can be obtained by linearly adding the field shown in Figs. 7a and c with an amplitude modulation of $\sqrt{2}/2$, the resonance in Fig. 7b is enhanced. Similarly, the field at $\psi = 135°$ can be obtained by linearly adding the field shown in Fig. 7c with an amplitude modulation of $\sqrt{2}/2$ and the field for $\psi = 180°$ with the same amplitude modulation. Since the field for $\psi = 180°$ is pointing to the opposite direction compared with Fig. 7a, the magnetic fields cancel out with each other and resonance effect is suppressed at $\psi = 135°$ as shown in Fig. 7d. This is the reason why at $\lambda = 5.70$ μm the emittance peak is maximized at $\psi = 45°$. Similar explanation can be applied to understand the polarization dependence at $\lambda = 8.13$ μm. However, at this wavelength, the magnetic fields in Figs. 7e and 7g, which correspond to $\psi = 0°$ and 90°, respectively, are generally pointing to opposite directions. Also, the magnetic field which correspond to $\psi = 90°$ (Fig. 7g) and the case for $\psi = 180°$, respectively, are pointing to the same direction, resulting in that the resonance is enhanced at the polarization angle of 135° (Fig. 7h) but annihilated when the polarization angle is 45° (Fig. 7f). Therefore, the emittance peak is maximized at $\psi = 135°$ for $\lambda = 8.13$ μm. Another explanation for the polarization dependence is the in-phase and anti-phase electromagnetic resonances as shown in Fig. 8, which depicts the time-dependent normalized amplitude of the magnetic field in the middle of dielectric spacer. Since a pulse source in the time domain is used in the simulation, the resonances are built after 200 fs. After 200 fs, the resonance for different

Please cite this article as: Sakurai A, et al. Effect of polarization on dual-band infrared metamaterial emitters or absorbers. J Quant Spectrosc Radiat Transfer (2015), http://dx.doi.org/10.1016/j.jqsrt.2014.11.018

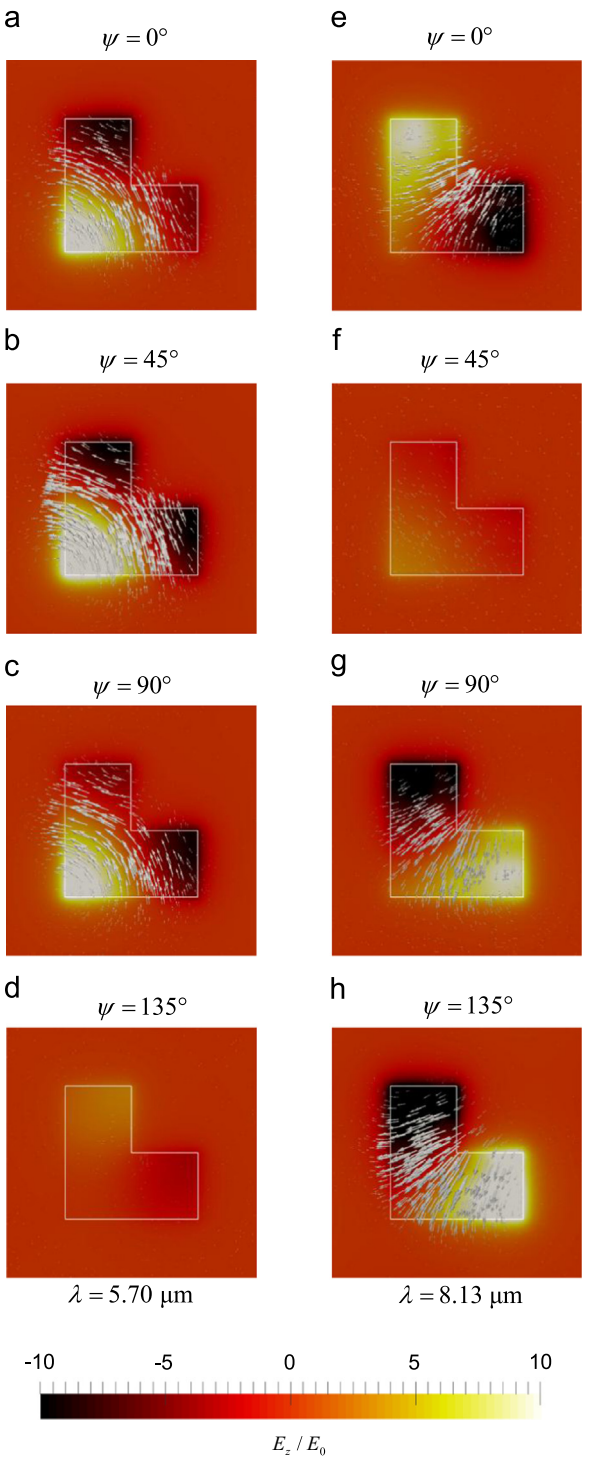

Fig. 7. Electric field contour at each resonant wavelength in the middle plane of the dielectric spacer with varying polarization angles. The contour shows the relative magnitude of the z component of the electric field. The arrows show the direction and magnitude of the magnetic field: (a) ψ=0°, (b) ψ=45°, (c) ψ=90°, and (d) ψ=135° at λ=5.70 μm; (e) ψ=0°, (f) ψ=45°, (g) ψ=90°, and (h) ψ=135° at λ=8.13 μm.

polarization shows the in-phase and anti-phase feature. For λ=8.13 μm, it is clearly observed that the magnetic

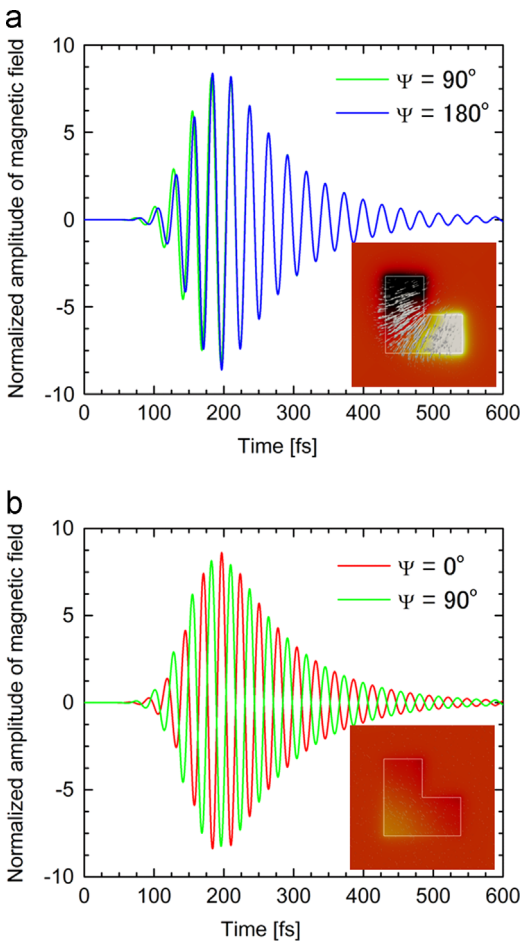

Fig. 8. Time-dependent normalized amplitude of magnetic field at the center of the dielectric spacer: (a) the in-phase response and (b) the anti-phase response.

field for the cases $\psi = 90°$ and 180° are in-phase response (Fig. 8a), on the other hand, the magnetic field for the cases $\psi = 0°$ and 90° are anti-phase response (Fig. 8b). Therefore, the resonances are enhanced by the in-phase response and annihilated by the anti-phase response. These interference effects and the existence of the eigen-polarization states for each wavelength have been also discussed in detail by Zhao et al. [31]. The polarization angles $\psi = 45°$ and 135° are the eigenpolarization in the considered L-shape pattern metamaterial. For other polarization angles, the resonance magnitude falls in between the maximum and minimum cases.

For the L-shape pattern metamaterial, the two resonances at λ=5.70 μm and 8.13 μm can be attributed to the MPs. However, the electromagnetic fields are different from MPs in the metamaterial with double-rectangle patterns as shown in Fig. 7. For wavelength λ=5.70 μm and $\psi = 45°$ (Fig. 7b), the magnetic field is curved along the diagonal. For wavelength λ=8.13 μm and $\psi = 135°$ (Fig. 7h), the magnetic field along the diagonal can also be observed. Therefore, all the parameters used in Eq. (1) have to be reevaluated for the L-shape metamaterial based on the field distribution at resonances. For the resonant

Please cite this article as: Sakurai A, et al. Effect of polarization on dual-band infrared metamaterial emitters or absorbers. J Quant Spectrosc Radiat Transfer (2015), http://dx.doi.org/10.1016/j.jqsrt.2014.11.018

wavelength $\lambda=5.70$ μm, the modified mutual and kinetic inductance and capacitance can be evaluated as

$$L_m = \frac{1}{2}\mu_0 \frac{(\sqrt{2}/2)w_1 d}{(\pi/4)w_1} = \frac{\sqrt{2}}{\pi}\mu_0 d \tag{3}$$

$$L_k = -\frac{(\sqrt{2}/2)w_1}{\varepsilon_0\omega^2(\pi/4)w_1\delta}\frac{\varepsilon'}{(\varepsilon'^2+\varepsilon''^2)} = -\frac{2\sqrt{2}}{\pi\varepsilon_0\omega^2\delta}\frac{\varepsilon'}{(\varepsilon'^2+\varepsilon''^2)} \tag{4}$$

$$C_m = c'\varepsilon_d\varepsilon_0\frac{3w_1^2}{4d} \tag{5}$$

For the inductance calculation, the length l is assumed to be curved along the diagonal, and also the characteristic length w is defined along the diagonal. For the capacitance, the area of L-shape pattern is simply calculated 3/4 of w_1^2. Note that the relationship $w_1 = 2w_2$ has been used to obtain Eqs. (3)–(5). For the resonant wavelength $\lambda=8.13$ μm, the modified parameters can be expressed as

$$L_m = \frac{1}{2}\mu_0 \frac{\sqrt{2}w_1 d}{(\sqrt{2}/2)w_1} = \mu_0 d \tag{6}$$

$$L_k = -\frac{\sqrt{2}w_1}{\varepsilon_0\omega^2(\sqrt{2}/2)w_1\delta}\frac{\varepsilon'}{(\varepsilon'^2+\varepsilon''^2)} = -\frac{2}{\varepsilon_0\omega^2\delta}\frac{\varepsilon'}{(\varepsilon'^2+\varepsilon''^2)} \tag{7}$$

$$C_m = c'\varepsilon_d\varepsilon_0\frac{3w_1^2}{4d} \tag{8}$$

Since the mainstream of magnetic field is not curved, the characteristic lengths can be defined along the diagonals. The optimized parameters c' for the L-shape pattern metamaterial can be obtained as 0.253 and 0.231 for fitting the resonant wavelengths $\lambda=5.70$ μm and 8.13 μm, respectively. Consequently, this explanation with the LC circuit model is valid for the L-shape metamaterial. Thus, the two emittance peaks are due to two different modes of MPs.

4. Conclusions

The spectral radiative properties of metamaterials made of either double-rectangle or L-shape gold pattern are investigated based on FDTD simulations. Dual-band emission or absorption peaks can be achieved in the infrared region from both structures and can be explained by magnetic resonances quantitatively using the LC circuit model considering the particular geometry and field distributions in each structure. For the two disconnected rectangular patterns, polarization insensitivity can be obtained at normal emittance. However, strong near-field coupling or interference can occur in the L-shape patterned metamaterial, resulting in polarization selectivity of the individual emission peaks. The underlying mechanisms are illustrated with the field distributions. The knowledge gained from this work may benefit the design of wavelength-selective multi-band emitters or absorbers that are either polarization independent or polarization selective.

Acknowledgments

This work was supported by the National Science Foundation (CBET-1235975).

References

[1] Fu CJ, Zhang ZM. Thermal radiative properties of metamaterials and other nanostructured materials: a review. Front Energy Power Eng China 2009;3:11–26.
[2] Watts CM, Liu XL, Padilla WJ. Metamaterial electromagnetic wave absorbers. Adv Mater 2012;24:OP98–120.
[3] Pendry JB, Holden AJ, Robbins DJ, Stewart WJ. Magnetism from conductors and enhanced nonlinear phenomena. IEEE Trans Microw Theory Tech 1999;47:2075–84.
[4] Liu XL, Tyler T, Starr T, Starr AF, Jokerst NM, Padilla WJ. Taming the blackbody with infrared metamaterials as selective thermal emitters. Phys Rev Lett 2011;107:045901.
[5] Landy NI, Sajuyigbe S, Mock JJ, Smith DR, Padilla WJ. Perfect metamaterial absorber. Phys Rev Lett 2008;100:207402.
[6] Aydin K, Ferry VE, Briggs RM, Atwater HA. Broadband polarization-independent resonant light absorption using ultrathin plasmonic super absorbers. Nat Commun 2011;2:517.
[7] Wang LP, Zhang ZM. Wavelength-selective and diffuse emitter enhanced by magnetic polaritons for thermophotovoltaics. Appl Phys Lett 2012;100:063902.
[8] Zhao B, Wang LP, Shuai Y, Zhang ZM. Thermophotovoltaic emitters based on a two-dimensional grating/thin-film nanostructure. Int J Heat Mass Transf 2013;67:637–45.
[9] Wu CH, Khanikaev AB, Adato R, Arju N, Yanik AA, Altug H, et al. Fano-resonant asymmetric metamaterials for ultrasensitive spectroscopy and identification of molecular monolayers. Nat Mater 2012;11:69–75.
[10] Liu N, Mesch M, Weiss T, Hentschel M, Giessen H. Infrared perfect absorber and its application as plasmonic sensor. Nano Lett 2010;10:2342–8.
[11] Zhang BX, Zhao YH, Hao QZ, Kiraly B, Khoo IC, Chen SF, et al. Polarization-independent dual-band infrared perfect absorber based on a metal–dielectric–metal elliptical nanodisk array. Opt Express 2011;19:15221–8.
[12] Tao H, Bingham CM, Pilon D, Fan KB, Strikwerda AC, Shrekenhamer D, et al. A dual band terahertz metamaterial absorber. J Phys D – Appl Phys 2010;43:225102.
[13] Chen K, Adato R, Altug H. Dual-band perfect absorber for multispectral plasmon-enhanced infrared spectroscopy. ACS Nano 2012;6:7998–8006.
[14] Montelongo Y, Tenorio-Pearl JO, Milne WI, Wilkinson TD. Polarization switchable diffraction based on subwavelength plasmonic nanoantennas. Nano Lett 2013;14:294–8.
[15] Syrenova S, Wadell C, Langhammer C. Shrinking-hole colloidal lithography: self-aligned nanofabrication of complex plasmonic nanoantennas. Nano Lett 2014;14:2655–63.
[16] Grady NK, Heyes JE, Chowdhury DR, Zeng Y, Reiten MT, Azad AK, et al. THz metamaterials for linear polarization conversion and anomalous refraction. Science 2013;340:1304–7.
[17] Black L-J, Wang YD, de Groot CH, Arbouet A, Muskens OL. Optimal polarization conversion in coupled dimer plasmonic nanoantennas for metasurfaces. ACS Nano 2014;8:6390–9.
[18] Canfield BK, Kujalal S, Jefimovs K, Vallius T, Turunen J, Kauranen M. Polarization effects in the linear and nonlinear optical responses of gold nanoparticle arrays. J Opt A – Pure Appl Opt 2005;7:S110–7.
[19] Yang J, Zhang J-S, Wu X-F, Gong Q-H. Resonant modes of L-shaped gold nanoparticles. Chin Phys Lett 2009;26:067802.
[20] Husu H, Mäkitalo J, Laukkanen J, Kuittinen M, Kauranen M. Particle plasmon resonances in L-shaped gold nanoparticles. Opt Express 2010;18:16601–6.
[21] Palik ED. Handbook of optical constants of solids, vol. I and vol. II. San Diego, CA: Academic Press; 1997.
[22] Zhang ZM. Nano/microscale heat transfer. New York: McGraw-Hill; 2007.
[23] Lee BJ, Wang LP, Zhang ZM. Coherent thermal emission by excitation of magnetic polaritons between periodic strips and a metallic film. Opt Express 2008;16:11328–36.
[24] Wang LP, Zhang ZM. Phonon-mediated magnetic polaritons in the infrared region. Opt Express 2011;19:A126–35.
[25] Wang LP, Haider A, Zhang ZM. Effect of magnetic polaritons on the radiative properties of inclined plate arrays. J Quant Spectrosc Radiat Transf 2014;132:52–60.

Please cite this article as: Sakurai A, et al. Effect of polarization on dual-band infrared metamaterial emitters or absorbers. J Quant Spectrosc Radiat Transfer (2015), http://dx.doi.org/10.1016/j.jqsrt.2014.11.018

[26] Engheta N. Circuits with light at nanoscales: optical nanocircuits inspired by metamaterials. Science 2007;317:1698–702.
[27] Zhou J, Economon EN, Koschny T, Soukoulis CM. Unifying approach to left-handed material design. Opt Lett 2006;31:3620–3622.
[28] Sakurai A, Zhao B, Zhang ZM. Prediction of the resonance condition of metamaterial emitters and absorbers using LC circuit model. In: Proceedings of the 15th international heat transfer conference, IHTC15-9012; 2014. p. 1–10.
[29] Sakurai A, Zhao B, Zhang ZM. Resonant frequency and bandwidth of metamaterial emitters and absorbers predicted by an RLC circuit model. J Quant Spectrosc Radiat Transf 2014;149:33–40.
[30] Zhao B, Zhang ZM. Study of magnetic polaritons in deep gratings for thermal emission control. J Quant Spectrosc Radiat Transf 2014;135:81–9.
[31] Zhao B, Sakurai A, Zhang ZM. Polarization dependence of the reflectance and transmittance of anisotropic metamaterials. AIAA J Thermophys Heat Transf (Forthcoming).

Please cite this article as: Sakurai A, et al. Effect of polarization on dual-band infrared metamaterial emitters or absorbers. J Quant Spectrosc Radiat Transfer (2015), http://dx.doi.org/10.1016/j.jqsrt.2014.11.018